Smooth objectives composed of asymptotically affine data-fidelity and regularization. Bounds for the minimizers and parameter choice

F. Baus, Mila Nikolova, Gabriele Steidl

Smooth objectives composed of asymptotically affine data-fidelity and regularization. Bounds for the minimizers and parameter choice

F. Baus, M. Nikolova, and G. Steidl

July 19, 2012

Abstract

We examine properties of the minimizer $\hat{u}$ of a class of differentiable functionals where both the data-term and the regularization term are symmetric and nearly affine beyond a small neighborhood of the origin. Customarily, such functions are used to regularize a quadratic data-fidelity term in order to produce solutions where edges are preserved. The functionals we consider in this paper behave quite differently. They were recently successfully applied to provide a strict order for the pixels of digital (quantized) images f thus enabling exact histogram specification. We give upper and lower bounds for the error $\|\hat{u} - f\|_\infty$, where the upper bound is independent of the input image f. Interestingly, in the numerical experiments with natural digital images f, the estimated upper bound is easily reached up to a small error. To explain this phenomenon we give simple statistical estimates for the behavior of neighboring pixels. We apply our estimates to specify the parameters of the model.

1 Introduction

In [9] a variational method using differentiable functionals where both the data-term and the regularization terms are symmetric and nearly linear beyond a small neighborhood of the origin was proposed. The goal was to process digital (quantized) images so that the obtained minimizer is quite close to the input digital image but its pixels are real-valued and can be ordered in a strict way. Indeed, the obtained minimizers were shown to enable faithful *exact histogram specification* outperforming the state-of-the-art methods [6, 10]. The intuition behind the conception of these functionals was also that their minimizer can up to some degree remove some quantization noise and in this way yield an ordering of the pixels close to the unknown original real-valued image. Such an effect can be observed in Fig. 1 where a synthetic real-valued image is quantized and then restored using the proposed variational method. This functional can also be seen as a fully smoothed version of the $L1 - TV$ model, studied originally in [4]. However, it was shown in [9] that its minimizers have a *qualitatively* different behavior: unlike the $L1 - TV$ minimizers, generically there are no pixels equal to those of the input image and there are no equally valued pixels.

Some of the authors of [9] observed that once the parameters of the model were fixed, for all kind of real-world digital images f, the residual error obeyed $\|\hat{u} - f\|_\infty = C$ where the constant C typically met $C < 0.5$. For this reason, they qualified this variational approach as *detail preserving*. It is worth to remained that such nearly linear functionals, known as *edge-preserving*, are customarily used along with a quadratic term in order to maintain edges in the restored images, see, e.g., [1, 2]. The latter are quite well understood and the literature is abundant; in particular, minimizers cannot satisfy $\|\hat{u}-f\|_\infty = C$ for a certain number of different input images f. Even though the model modification proposed in [9] might be seemingly trivial, the relevant minimizers obviously exhibit a qualitatively different behavior. Therefore we were interested in monitoring the error $\|\hat{u} - f\|_\infty$. We have computed the minimizer of the proposed

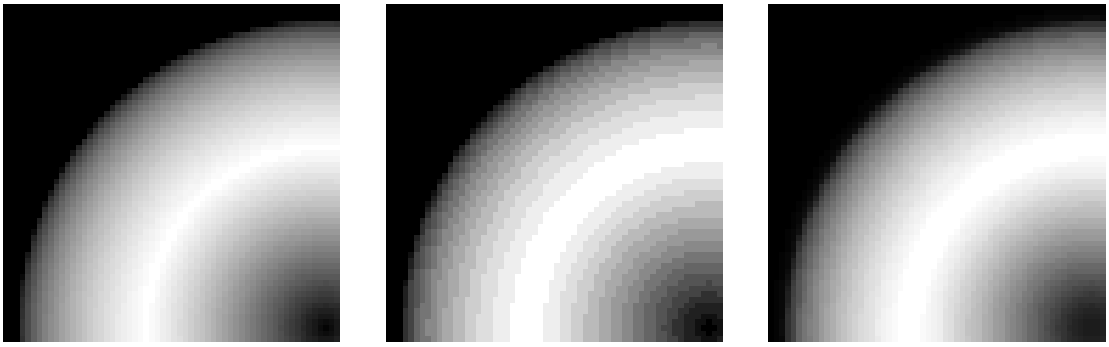

Real-valued image f—quantized on $\{0, \cdots, 15\}$ Restored $\hat{u}$

Figure 1: The restored image is obtained by minimizing $J(\cdot, f)$ of the form (1) where $\psi(t) = \sqrt{t^2 + \alpha_1}$ and $\varphi(t) = \sqrt{t^2 + \alpha_2}$ for $\mathcal{N}8$.

functionals for various parameter settings and a wide variety of digital input images of different sizes and with disparate content. The observation that $\|\hat{u} - f\|_\infty = C$, up to a very small difference, is independent of the input image, was confirmed. In this paper, we will give an explanation for this behavior which also enables us to give restrictions on the choice of the parameters involved in the model.

The outline of this paper is as follows: In the next Section 2 we review the variational model. Then, in Section 3 we estimate the ℓ_∞-error between the input image f and the minimizer of the functional. Section 4 provides explicit parameter estimates for the model. In Section 5 we give probability estimates for the behavior of neighboring pixels. Numerical tests demonstrate the quality of our estimates in Section 6. Finally, Section 7 finishes with conclusions.

2 The Fully Smoothed ℓ_1-TV Model

We consider $M \times N$ digitized images f with gray values in $\{0, \ldots, L-1\}$. Let $n := MN$. To simplify the notation we reorder the image columnwise into a vector of size n and address the pixels by the index set $\mathbb{I}_n := \{1, \cdots, n\}$. Further, we denote by $\mathbb{I}_n^{\text{int}} \subset \mathbb{I}_n$ the subset of all inner pixels, i.e., all pixels which are not boundary pixels.

We are interested in the minimizer $\hat{u}$ of a functional of the form

$$J(u, f) := \Psi(u, f) + \beta\Phi(u), \quad \beta > 0 \tag{1}$$

with

$$\begin{aligned} \Psi(u, f) &:= \sum_{i \in \mathbb{I}_n} \psi(u[i] - f[i]), \\ \Phi(u) &:= \sum_{i \in \mathbb{I}_n} \sum_{j \in \mathcal{N}_i} \varphi(\gamma_{i,j}(u[i] - u[j])) \ , \end{aligned}$$

where $\mathcal{N}_i$ is a neighborhood of pixel i, the $\gamma_{i,j} > 0$ are weighting terms for the distance between neighbors, and the functions ψ and φ are nearly affine beyond a small neighborhood of the origin. Both ψ and φ depend on a positive parameter, α_1 and α_2, respectively. To emphasize this dependence we use the notation $\psi(\cdot, \alpha_1)$ and $\varphi(\cdot, \alpha_2)$ when necessary. So $\psi : \mathbb{R} \times (0, +\infty) \to \mathbb{R}$ and $\varphi : \mathbb{R} \times (0, +\infty) \to \mathbb{R}$. The functions ψ and φ have to fulfill the properties stated below.

H0 The functions $t \mapsto \psi(t, \alpha_1)$ and $t \mapsto \varphi(t, \alpha_2)$ are continuously differentiable and even.

We denote

$$\psi'(t, \alpha_1) := \frac{d}{dt}\psi(t, \alpha_1) \quad \text{and} \quad \varphi'(t, \alpha_2) := \frac{d}{dt}\varphi(t, \alpha_2) \ .$$

When it is clear from the context, we write $\psi'(t)$ for $\psi'(t,\alpha_1)$ and $\varphi'(t)$ for $\varphi'(t,\alpha_2)$. By H0 , $\psi'(t)$ and $\varphi'(t)$ are continuous and odd functions.

These derivative functions have to satisfy certain conditions given next.

H1$^\psi$ $\psi' : \mathbb{R} \to (-Y, Y)$, where $Y > 0$, is a strictly increasing function which maps onto $(-Y, Y)$.

H2$^\psi$ There is a constant $T > 0$ such that for any fixed $t \in (0, T)$, the function $\alpha_1 \mapsto \psi'(t, \alpha_1)$ is strictly decreasing on $(0, +\infty)$.

Here the cases $T = +\infty$ and $Y = +\infty$ are included.

H1$^\varphi$ φ' is an increasing function satisfying

$$\lim_{t\to\infty} \varphi'(t) = 1.$$

H2$^\varphi$ For any fixed $t > 0$, the function $\alpha_2 \mapsto \varphi'(t, \alpha_2)$ is continuous and decreasing on $(0, +\infty)$ and

$$\lim_{\alpha_2\to 0} \varphi'(t, \alpha_2) = 1.$$

These properties imply further useful relations which are collected in the following remark.

Remark 1 i) *By* H1$^\psi$ *we know that ψ is strictly convex and monotone increasing on* $(0, +\infty)$ *and by* H1$^\varphi$ *that φ is convex. Therefore there exists a unique minimizer of* (1). *This minimizer can be computed, e.g., by using a Weiszfeld-like semi-implicit algorithm, or the nonlinear (preconditioned) conjugate gradient method, see* [5, 9, 11].

ii) *By* H1$^\psi$ *there exists the inverse function $(\psi')^{-1} : (-Y, Y) \to \mathbb{R}$, and this function is also odd, continuous and strictly increasing.*

Some relevant choices of functions θ obeying both H1$^\psi$, H2$^\psi$ and H1$^\varphi$, H2$^\varphi$ are given in Table 1. Here the functions θ' map onto $(-1, 1)$, i.e., $Y = 1$ and $T = +\infty$ A typical graph of such a function, its derivative and inverse derivative is depicted in Fig. 2.

	θ	θ'	$(\theta')^{-1}$
$\Theta 1$	$\sqrt{t^2+\alpha}$	$\dfrac{t}{\sqrt{t^2+\alpha}}$	$y\sqrt{\dfrac{\alpha}{1-y^2}}$
$\Theta 2$	$\lvert t\rvert - \alpha \log\left(1 + \dfrac{\lvert t\rvert}{\alpha}\right)$	$\dfrac{t}{\alpha + \lvert t\rvert}$	$\dfrac{\alpha y}{1-\lvert y\rvert}$
$\Theta 3$	$\alpha \log\left(\cosh\left(\dfrac{t}{\alpha}\right)\right)$	$\tanh\left(\dfrac{t}{\alpha}\right)$	$\alpha\,\mathrm{atanh}(y)$

Table 1: Options for functions θ obeying all the assumptions stated above. The size of the neighborhood of zero where these functions are not nearly affine is controlled by the parameter $\alpha > 0$.

Another relevant choice for ψ is the *scaled ℓ_p-norm*:

$$\psi(t) := \frac{1}{\alpha_1 + 1} |\, t \,|^{\alpha_1+1} \quad \text{with} \quad \psi'(t) = |\, t \,|^{\alpha_1}\mathrm{sign}(t), \quad (\psi')^{-1}(y) = |\, y \,|^{\frac{1}{\alpha_1}}, \quad \alpha_1 > 0. \tag{2}$$

Here ψ' maps onto $\mathbb{R}$ so that $Y = +\infty$. Moreover $\alpha_1 \mapsto \psi'(t, \alpha_1)$ is strictly monotone decreasing for $|t| < 1$ so that $T = 1$ here.

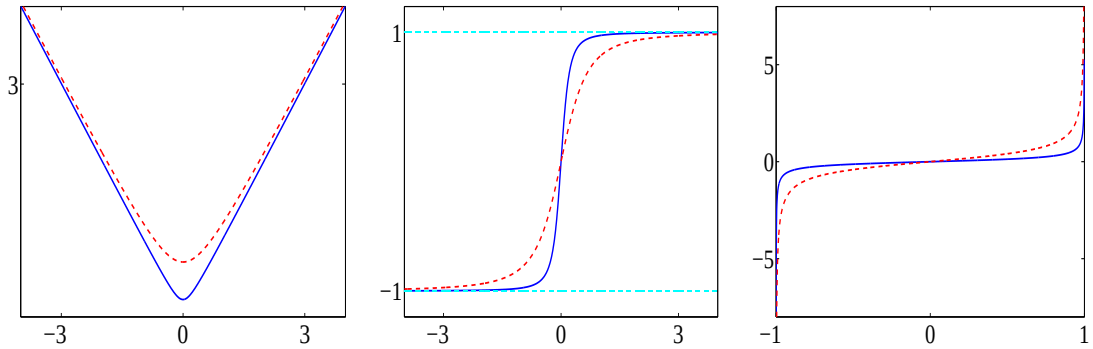

Figure 2: The function Θ1 in Table 1, where the plots for $\alpha = 0.05$ are in blue solid line and for $\alpha = 0.5$—in red dashed line.

For φ we can also use the *scaled Huber function*

$$\varphi(t) := \begin{cases} \dfrac{t^2}{2\alpha_2} & \text{if} \quad |t| \leqslant \alpha_2, \\ |t| - \dfrac{\alpha_2}{2} & \text{if} \quad |t| > \alpha_2 \end{cases} \qquad \text{with} \quad \varphi'(t) = \begin{cases} \dfrac{t}{\alpha_2} & \text{if} \quad |t| \leqslant \alpha_2, \\ \operatorname{sign}(t) & \text{if} \quad |t| > \alpha_2. \end{cases} \tag{3}$$

In this paper, we focus on the neighborhoods $\mathcal{N}4$ and $\mathcal{N}8$ depicted in Fig. 3 top. When taking the gradient of the functional in (1) we have to take into account that the pixel combinations $u[i] - u[j]$ appears for $j \in \mathcal{N}_i^2$, where $\mathcal{N}_i^2$ denotes the 'double' neighborhood associated with $\mathcal{N}_i$ in Fig. 3 bottom. The usual choices are (see e. g. [7])

$$\begin{aligned} \gamma_{i,j} &:= 1 && \text{for vertical and horizontal neighbors,} \\ \gamma_{i,j} &:= \frac{1}{\sqrt{2}} && \text{for diagonal neighbors.} \end{aligned} \tag{4}$$

In all cases we have $\gamma_{i,j} = \gamma_{j,i}$.

Functionals of the form (1) with functions $\psi, \varphi \in \mathcal{C}^s$, $s \geq 2$ having certain properties were successfully used in [9] to process digital images f so that the obtained minimizer $\hat{u}$ is quite close to the input digital image but its pixels can be ordered in a strict way. An analysis of the minimizers $\hat{u}$ of these functionals has shown that almost surely, $\hat{u}$ has pixel values that are different from each other and different from the input pixels.

3 Bounds for the ℓ_∞-Error

In this section, we give upper and lower estimates for the ℓ_∞-error between the input image f and the image $\hat{u}$ obtained by minimizing the functional $J(\cdot, f)$.

If $\hat{u}$ is a minimizer of $u \mapsto J(u, f)$ we denote by $h \in \mathbb{R}^n$ the vector with components

$$h[i] := \sum_{j \in \mathcal{N}_i^2} \gamma_{i,j} \varphi' \left(\gamma_{i,j} (\hat{u}[i] - \hat{u}[j]) \right), \quad i \in \mathbb{I}_n. \tag{5}$$

First we provide a lemma which gives a useful expression for $\|\hat{u} - f\|_\infty$.

Lemma 1 *Let* H0 , H1$^\psi$ *and* H1$^\varphi$ *be satisfied. Let* $\hat{u}$ *be the minimizer of* $u \mapsto J(u, f)$ *and* h *be given by* (5). *Then*

$$\|\hat{u} - f\|_\infty = (\psi')^{-1} \left(\beta \, \| \, h \, \|_\infty \right) \ . \tag{6}$$

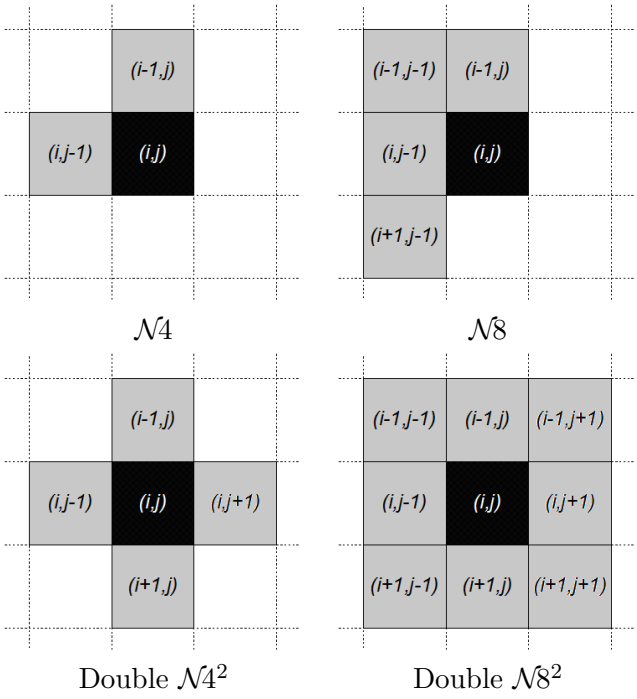

Figure 3: Neighborhoods $\mathcal{N}4$ and $\mathcal{N}8$ (right) of a pixel (i,j) are used to formulate $\Phi(u)$. The double neighborhoods $\mathcal{N}4^2$ and $\mathcal{N}8^2$ appear in the gradient of $\Phi(u)$, see (7).

Proof. By definition of J and taking into account that φ' is odd, we have

$$\frac{\partial \Psi}{\partial u[i]} = \psi'(u[i] - f[i]) \quad \text{and} \quad \frac{\partial \Phi}{\partial u[i]} = \sum_{j \in \mathcal{N}_i^2} \gamma_{i,j} \varphi'(\gamma_{i,j}(u[i] - u[j])) \; . \tag{7}$$

The minimizer $\hat{u}$ of $J(\cdot, f)$ has to satisfy $\nabla_u J(\hat{u}, f) = 0$ which can be rewritten as $\nabla_u \Psi(\hat{u}, f) = -\beta \nabla \Phi(\hat{u})$ or as

$$\psi'(\hat{u}[i] - f[i]) = -\beta \sum_{j \in \mathcal{N}_i^2} \gamma_{i,j} \varphi'(\gamma_{i,j}(\hat{u}[i] - \hat{u}[j])), \quad i \in \mathbb{I}_n.$$

Using (5), the latter is equivalent to

$$\psi'(\hat{u}[i] - f[i]) = -\beta \, h[i], \quad i \in \mathbb{I}_n.$$

Since ψ' is by H0 and H1$^\psi$ odd and strictly increasing,

$$\psi' \left(\left| \, \hat{u}[i] - f[i] \, \right| \right) = \left| \, \psi'(\hat{u}[i] - f[i]) \, \right| = \beta \left| \, h[i] \, \right| \; . \tag{8}$$

Using Remark 1ii), we see that (8) is equivalent to

$$\left| \, \hat{u}[i] - f[i] \, \right| = (\psi')^{-1} \left(\beta \left| \, h[i] \, \right| \right) \tag{9}$$

where $(\psi')^{-1}$ is strictly increasing, hence

$$\| \hat{u} - f \|_\infty = \max_{i \in \mathbb{I}_n} (\psi')^{-1} \left(\beta \left| \, h[i] \, \right| \right) = (\psi')^{-1} \left(\beta \, \| \, h \, \|_\infty \right) \; .$$

□

For inner points $i \in \mathbb{I}_n^{\text{int}}$ we define

$$\eta := \sum_{j \in \mathcal{N}_i^2} \gamma_{i,j}. \tag{10}$$

Of course η does not depend on i but just on the choice of the neighborhood. If the weighs are are defined as in (4), we have

$$\begin{aligned} \eta &= 4 && \text{for} \quad \mathcal{N}4, \\ \eta &= 4 + \frac{4}{\sqrt{2}} = 6.8284 && \text{for} \quad \mathcal{N}8. \end{aligned}$$

For $i \in \mathbb{I}_n \setminus \mathbb{I}_n^{\text{int}}$ we have $\sum_{j \in \mathcal{N}_i^2} \gamma_{i,j} \leqslant \eta$ whose value depends on the boundary conditions.

In order to extend the obtained result, we shall further use a property of $(\psi')^{-1}$ which is stated in the following lemma.

Lemma 2 *Let ψ satisfy* H0 , H1$^\psi$ *and* H2$^\psi$. *Set*

$$\widetilde{Y} := \min\{Y, \psi'(T)\} \ .$$

Then for any $y \in (0, \widetilde{Y})$, the function $\alpha_1 \mapsto (\psi')^{-1}(y, \alpha_1)$ is strictly increasing on $(0, +\infty)$.

Proof. Let $0 < \alpha_1 < \alpha_2$ and $y \in (0, \widetilde{Y})$ be arbitrarily fixed. Since $t \mapsto \psi'(t, \alpha)$ is one-to-one and odd, there exist $t_1, t_2 \in (0, T)$ such that

$$\psi'(t_1, \alpha_1) = y = \psi'(t_2, \alpha_2) \tag{11}$$

and thus $(\psi')^{-1}(y, \alpha_1) = t_1$ and $(\psi')^{-1}(y, \alpha_2) = t_2$. From H1$^\psi$, $t \mapsto \psi'(t, \alpha)$ is strictly increasing for fixed $\alpha > 0$ and from H2$^\psi$, $\alpha \mapsto \psi'(t, \alpha)$ is strictly decreasing for fixed $t \in (0, T)$. Therefore

$$t_2 \leqslant t_1 \quad \Rightarrow \quad y = \psi'(t_1, \alpha_1) > \psi'(t_1, \alpha_2) \geqslant \psi'(t_2, \alpha_2).$$

This contradicts (11). Consequently, $t_1 < t_2$ which implies the assertion. □

Note that $\widetilde{Y} = 1$ both for all functions in Table 1 and for ψ in (2).

The following theorem provides an upper bound for $||\hat{u} - f||_\infty$ which is independent of f as well as of the particular shape of $\varphi(t, \alpha_2)$ provided that the latter meets H1$^\varphi$.

Theorem 1 *Assume that* H0 , H1$^\psi$ *and* H1$^\varphi$ *are satisfied. Let $\beta\,\eta < Y$, where η is given in* (10). *Then the minimizer $\hat{u}$ of $u \mapsto J(u, f)$ fulfills*

$$\|\hat{u} - f\|_\infty \leq (\psi')^{-1}\big(\beta\eta, \alpha_1\big) := b(\beta, \alpha_1) \ . \tag{12}$$

If ψ fulfills in addition H2$^\psi$ *and $\beta\,\eta < \widetilde{Y}$, where $\widetilde{Y} = \min\{Y, \psi'(T)\}$, then $\alpha_1 \mapsto b(\beta, \alpha_1)$ is strictly increasing on $(0, +\infty)$.*

Note that equality in (12) can only be fulfilled if φ' attains the limit in H1$^\varphi$, i.e., if $\varphi'(t) = 1$ for some $t \in \mathbb{R}$. This is for example the case for the scaled Huber function in (3).

Proof. By definition of h and since φ' is increasing with $|\varphi'(t)| \leq 1$ for any $t \in \mathbb{R}$ we obtain

$$\|h\|_\infty \leq \eta. \tag{13}$$

Since $(\psi')^{-1}$ is by Remark 1ii) strictly increasing on $(0, Y)$, we deduce from (6) and (13) for $\beta\,\eta < Y$ that

$$\|\hat{u} - f\|_\infty = (\psi')^{-1}\,(\beta\,\|\,h\,\|_\infty) \leq (\psi')^{-1}\,(\beta\,\eta) \ .$$

Note that this bound depends only on ψ (and hence on α_1) and on β, so that the expression for the constant $b(\cdot)$ in (12) follows. If ψ fulfills H2$^\psi$ and $\beta\,\eta < \widetilde{Y}$ we obtain by Lemma 2 that the

function $\alpha_1 \mapsto (\psi')^{-1}\big(\beta\eta, \alpha_1\big)$ is strictly increasing on $(0, +\infty)$. $\square$

The lower bound on $\|\hat{u} - f\|_\infty$ exhibited in the next Theorem 2 depends on $\varphi(t, \alpha_2)$ and on the input image f as well. In our formula, the reliance on f is expressed *via* the magnitude ν_f defined below:

$$\begin{array}{rcl} \mathcal{I} & := & \big\{ i \in \mathbb{I}_n^{\rm int} \;\big|\; \mathrm{sign}\big(f[i] - f[j]\big) = \sigma,\ \forall\, j \in \mathcal{N}_i \ \text{ where } \ \sigma \in \{-1, +1\} \big\}\ , \\ \nu_f & = & \max\limits_{i \in \mathcal{I}} \min\limits_{j \in \mathcal{N}_i} \big(\gamma_{i,j} \,\big|\, f[i] - f[j] \,\big|\big)\ . \end{array} \tag{14}$$

The values of ν_f for some real-world images can be seen in Fig. 7.

Theorem 2 *We consider that* H0 , H1$^\psi$, H2$^\psi$ *and* H1$^\varphi$, H2$^\varphi$ *are verified. Let* $\beta\,\eta < Y$*, where* η *is given in* (10)*. Assume that* $\nu_f > 2b(\beta, \alpha_1)$*. Then the minimizer* $\hat{u}$ *of* $u \mapsto J(u, f)$ *fulfills*

$$\|\hat{u} - f\|_\infty \geqslant (\psi')^{-1}\,(c\,\beta\,\eta) := \ell(\beta, \alpha_1, \alpha_2, \nu_f)\ , \tag{15}$$

where

$$c = c\big(\beta, \alpha_1, \alpha_2, \nu_f\big) := \varphi'\Big(\nu_f - 2b(\beta, \alpha_1), \alpha_2\Big) \leqslant 1\ .$$

The function $\alpha_2 \mapsto \ell(\beta, \alpha_1, \alpha_2, \nu_f)$ *is decreasing on* $(0, +\infty)$ *and*

$$\ell(\beta, \alpha_1, \alpha_2, \nu_f) \nearrow b(\beta, \alpha_1) \quad as \quad \alpha_2 \searrow 0\ . \tag{16}$$

If in addition the image of $\alpha_2 \mapsto \varphi'(t, \alpha_2)$ *contains* $(0, 1)$*, then for any* $\varepsilon \in (0, 1)$ *there exists* $\alpha_2 > 0$ *such that*

$$\|\hat{u} - f\|_\infty \geqslant (\psi')^{-1}\,((1 - \varepsilon)\,\beta\,\eta)\ .$$

Proof. From the assumption on ν_f, there is $i \in \mathbb{I}_n^{\rm int}$ such that

$$\gamma_{i,j} \big|\ f[i] - f[j]\ \big| \geqslant \nu_f \ \ \forall\, j \in \mathcal{N}_i.$$

Assume that

$$\gamma_{i,j}(f[i] - f[j]) \geqslant \nu_f > 2b(\beta, \alpha_1), \quad \forall j \in \mathcal{N}_i. \tag{17}$$

The opposite case, namely $\gamma_{i,j}(f[j] - f[i]) \geqslant \nu_f > 2b(\beta, \alpha_1)$, $\forall\ j \in \mathcal{N}_i$ can be handled in the same way. By Theorem 1, the minimizer $\hat{u}$ of $J(\cdot, f)$ meets

$$\begin{array}{rcl} -b(\beta, \alpha_1) & \leqslant & \hat{u}[i] - f[i], \\ -b(\beta, \alpha_1) & \leqslant & f[j] - \hat{u}[j], \quad \forall j \in \mathcal{N}_i\ . \end{array}$$

Thus

$$\begin{array}{rcl} -2b(\beta, \alpha_1) & \leqslant & \hat{u}[i] - \hat{u}[j] - \big(f[i] - f[j]\big), \quad \forall j \in \mathcal{N}_i\ , \\ -2b(\beta, \alpha_1) + \big(f[i] - f[j]\big) & \leqslant & \hat{u}[i] - \hat{u}[j], \quad \forall j \in \mathcal{N}_i\ . \end{array} \tag{18}$$

Combining (17) and (18) along with the fact that $\gamma_{i,j} \leq 1$ yields

$$0 < -2b(\beta, \alpha_1) + \nu_f \leqslant -2b(\beta, \alpha_1) + \gamma_{i,j}(f[i] - f[j]) \leqslant \gamma_{i,j}(\hat{u}[i] - \hat{u}[j]) \quad \forall\, j \in \mathcal{N}_i\ .$$

Since φ' is increasing by H1$^\varphi$, the value $h[i]$ in (5) satisfies

$$h[i] \geqslant \sum_{j \in \mathcal{N}_i^2} \gamma_{i,j}\, \varphi'\Big(\nu_f - 2b(\beta, \alpha_1)\Big) = \eta\, c\big(\beta, \alpha_1, \alpha_2, \nu_f\big).$$

Using yet again that $(\psi')^{-1}$ is strictly increasing (Remark 1ii)) shows that $\big|\,\hat{u}[i]-f[i]\,\big|$ as given in (9) satisfies

$$\big|\,\hat{u}[i]-f[i]\,\big| \geq (\psi')^{-1}\,(c\,\beta\eta)\ .$$

Since $\|\hat{u}-f\|_\infty \geqslant \big|\,\hat{u}[i]-f[i]\,\big|$, it follows that

$$\|\hat{u}-f\|_\infty \geqslant (\psi')^{-1}\,(c\,\beta\eta)\ .$$

Using H2$^\varphi$, the function $\alpha_2 \mapsto c(\beta,\alpha_1,\alpha_2,\nu_f)$ is continuous and decreasing on $(0,+\infty)$ and $\lim\limits_{\alpha_2 \searrow 0} c(\beta,\alpha_1,\alpha_2,\nu_f) = 1$. Combining the latter with Remark 1ii) entails that $\alpha_2 \mapsto \ell(\beta,\alpha_1,\alpha_2,\nu_f)$ is decreasing on $(0,+\infty)$ and that (16) holds true given the definition of $b(\beta,\alpha_1)$ in (12).

Under the additional assumption that the image of $\alpha_2 \mapsto \varphi'(t,\alpha_2)$ contains $(0,1)$, H2$^\varphi$ shows that for shows that for any $\varepsilon \in (0,1)$ there is $\alpha_2 > 0$ such that $c(\beta,\alpha_1,\alpha_2,\nu_f) = (1-\varepsilon)$. We can hence write down that $\|\hat{u}-f\|_\infty \geqslant (\psi')^{-1}\,((1-\varepsilon)\,\beta\eta)$. □

A simple consequence of (18) in the proof of Theorem 2 is that if a difference in the input image meets $f[i]-f[j] > 2b(\beta,\alpha_1)$, then the restored difference $\hat{u}[i]-\hat{u}[j]$ remains positive.

For the Huber function in (3), it easy to see that there is α_2 such that $c(\beta,\alpha_1,\alpha_2,\nu_f) = 1$ and hence $\ell(\beta,\alpha_1,\alpha_2,\nu_f) = b(\beta,\alpha_1)$.

4 Explicit Parameter Estimates

In this section we want to use the error bounds from the previous section to give explicit parameter estimates of β, α_1 and α_2 for the functions ψ,φ mentioned in Section 2. For the functions ψ in Table 1 and in (2) we have $\widetilde{Y} = 1$. When the weights $\gamma_{i,j}$ are chosen as in (4), the assumption $\beta\eta < \widetilde{Y} = 1$ in Theorem 1 reads

$$\begin{aligned} &\beta < \tfrac{1}{4} = 0.25 && \text{for} \quad \mathcal{N}4, \\ &\beta < \tfrac{1}{6.8284} = 0.1464 && \text{for} \quad \mathcal{N}8. \end{aligned} \tag{19}$$

In the following we fix $\beta > 0$ such that $\beta < \dfrac{1}{\eta}$. For $\delta > 0$, let $\widehat{\alpha}_1$ be the solution of

$$b(\beta,\alpha_1) = (\psi')^{-1}(\beta\eta,\alpha_1) = \delta \tag{20}$$

Since $\alpha_1 \to b(\beta,\alpha_1)$ is by Theorem 1 strictly increasing, the optimal choice for α_1 is

$$\alpha_1 = \widehat{\alpha}_1\ .$$

By the same theorem, the relation $\|\hat{u}-f\|_\infty < \delta$ is valid for all $\alpha_1 > 0$ with $\alpha_1 < \widehat{\alpha}_1$. If $\delta = 0.5$ then $\hat{u}$ has the important property that it preserves the order of the pixel values in $f \in \{0,\ldots,L-1\}^n$. According to Theorem 1 and Theorem 2, the upper and bounds for $\|f-\hat{u}\|_\infty$ and the optimal value for α_1 as defined in (20) are given for the functions ψ in Table 1 and in (2) in the following Table 2:

The value c depends on φ and on f via ν_f. Given the input image f the constant ν_f can be easily computed. Whenever

$$z := \nu_f - 2b(\beta,\alpha_1) > 0,$$

we obtain the constant c by

$$c = \varphi'(z). \tag{21}$$

By Theorem 2 a sharper lower bound requires a smaller value for α_2.

The allowed values for β according to Theorem 1 are given in (19). For $b(\beta,\alpha_1) = \delta > 0$ and β fixed we have established the upper values $\widehat{\alpha}_1$. For $\delta = 0.5$ these values are presented in Table 3.

$\psi(t)$	$b(\beta,\alpha_1)$	$\ell(\beta,\alpha_1,\alpha_2,\nu_f)$	$\widehat{\alpha}_1$
$\sqrt{t^2+\alpha_1}$	$\sqrt{\frac{\alpha_1(\beta\eta)^2}{1-(\beta\eta)^2}}$	$\sqrt{\frac{\alpha_1(c\beta\eta)^2}{1-(c\beta\eta)^2}}$	$\delta^2\left(\frac{1}{\beta^2\eta^2}-1\right)$
$\lvert t\rvert-\alpha_1\log\left(1+\frac{\lvert t\rvert}{\alpha_1}\right)$	$\frac{\alpha_1\,\beta\eta}{1-\beta\eta}$	$\frac{\alpha_1\,c\beta\eta}{1-c\beta\eta}$	$\delta\left(\frac{1}{\beta\eta}-1\right)$
$\alpha\log\left(\cosh\left(\frac{t}{\alpha}\right)\right)$	$\alpha_1\,\mathrm{atanh}(\beta\eta)$	$\alpha_1\,\mathrm{atanh}(c\beta\eta)$	$\frac{\delta}{\mathrm{atanh}(\beta\eta)}$
$\frac{1}{\alpha_1+1}\lvert t\rvert^{\alpha_1+1}$	$\frac{1}{\alpha_1}(\beta\eta)^{\frac{1}{\alpha_1}}$	$\frac{1}{\alpha_1}(c\beta\eta)^{\frac{1}{\alpha_1}}$	$\frac{\ln(\beta\eta)}{\ln\delta}$

Table 2: Bounds and parameter $\widehat{\alpha}_1$ for various functions ψ in Table 1 and in (2). The parameter c depends on φ' by (21).

$\psi(t)$	$\sqrt{t^2+\alpha_1}$		$\lvert t\rvert-\alpha_1\log\left(1+\frac{\lvert t\rvert}{\alpha_1}\right)$	
neighborhood	β	$\widehat{\alpha}_1$	β	$\widehat{\alpha}_1$
$\mathcal{N}4$	0.2	0.1406	0.2	0.1250
$\mathcal{N}4$	0.1	1.3125	0.1	0.7500
$\mathcal{N}8$	0.1	0.2862	0.1	0.2322
$\mathcal{N}8$	0.05	1.8947	0.05	0.9645

Table 3: Allowed values $\beta < 1/\eta$ and the maximal $\widehat{\alpha}_1$ leading to $\delta = b(\beta,\hat{\alpha}_1) = 0.5$.

5 Probability Estimates for Pixel Neighborhoods

Let us assume that our digital images f are realizations of a discrete random variable X taking values in $\{0,\ldots,L-1\}$ with probability density function p_X. Fig. 4 shows an image together with its histogram as approximation of the probability density function of the corresponding random variable.

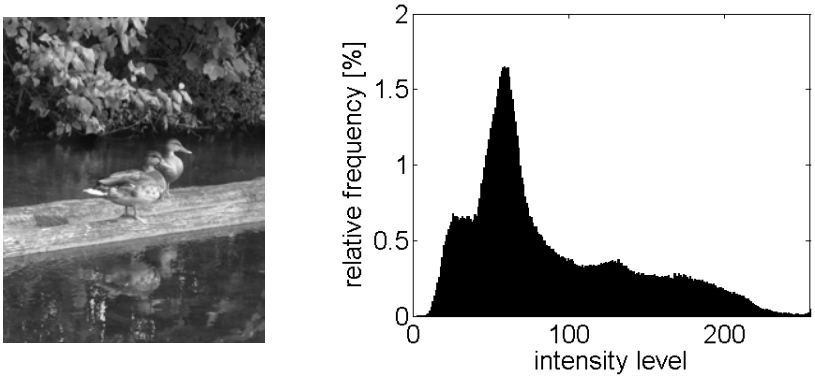

Figure 4: Left: Duck image. Right: Histogram of 'duck image'.

First, we ask for the probability that an inner image pixel $i \in \mathbb{I}_n^{\mathrm{int}}$ fulfills

$$\big|\, f[i]-f[j]\,\big| \geq a \quad \text{and} \quad \mathrm{sign}(f[i]-f[j]) = \sigma, \quad \forall j \in \mathcal{N}_i \tag{22}$$

where $\sigma \in \{-1,+1\}$ for some fixed $a > 0$.

Lemma 3 *Let X, X_i, $i = 1,\ldots,k$ be independent and identically distributed (iid) discrete ran-*

dom variables taking values in $\{0,\dots,L-1\}$. *Then it holds for* $a>0$ *that*

$$q(X,k,a) := P(X-X_1\geq a,\dots,X-X_k\geq a) = \sum_{i=0}^{L-1} \left(P(X\leq i-a)\right)^k P(X=i). \tag{23}$$

Proof. Since the random variables are iid we obtain

$$\begin{aligned} P(X-X_1\geq a,\dots,X-X_k\geq a) &= \sum_{i=0}^{L} \left(P(i-X_1\geq a,\dots,i-X_1\leq a, X=i)\right. \\ &= \sum_{i=0}^{L} \left(P(X\leq i-a)\right)^k P(X=i). \qquad \square \end{aligned}$$

The setting of Lemma 3 is stated for neighborhoods where the central pixel is not smaller than all its neighbors with distance at least a. Of course the opposite setting that the central pixel is not larger than all its neighbors with distance at least a is of the same interest and appears with the same probability $P(X-X_1\leq -a,\dots,X-X_k\leq -a) = q(X,k,a)$.

Example 1 *For* $k=1$, *i.e., just one neighbor pixel, the probabilities* $P(X-X_1\geq a)$ *and* $P(X-X_1\leq -a)$ *can be easily exemplified: compute the joint probability distribution of* X *and* X_1 *and add the probabilities of all points for which the difference is larger or equal to* a. *In Fig. 5 (left) all values in the shaded areas have to be summed up to obtain* $2q(X,1,a)$. *Fig. 5 (right) shows the approximate joint probability distribution of two iid random variables having the probability distribution of of the "ducks image" in Fig. 4. For uniformly i.i.d. random*

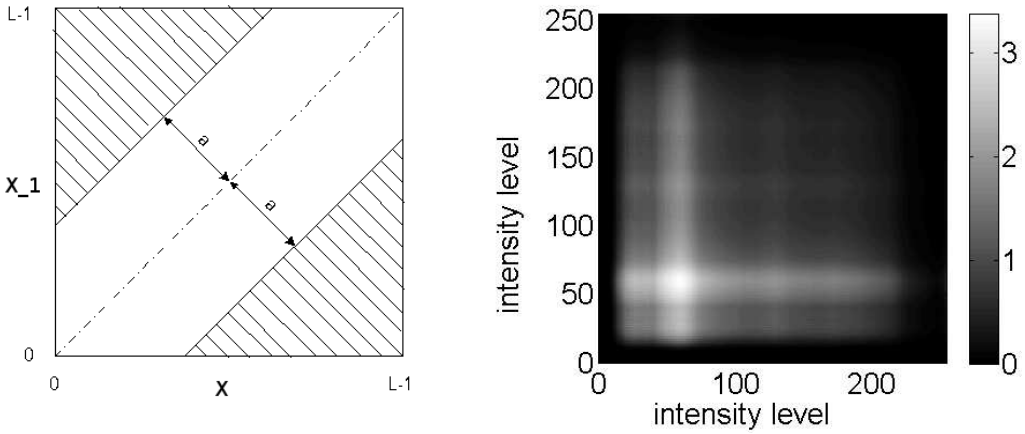

Figure 5: Left: Sketch of a joint probability density function of X and X_1. The value $2q(X,1,a)$ is the sum of the probabilities in the shaded areas. Right: Approximate joint probability distribution of two iid random variables having the probability distribution of of the "ducks image" in Fig. 4. The values of the color bar have to be scaled by 10^{-4}.

variables with values in $\{0,\dots,L-1\}$, *we obtain for a 4-neighborhood, i.e.,* $k=4$ *and* $a\in\mathbb{N}$ *for example*

$$q(X,4,a) = \frac{1}{L}\sum_{i=a}^{L-1}\left(\frac{i-a+1}{L}\right)^4 = \frac{(L-a)(L-a+1)(2(L-a)+1)(3(L-a)^2+3(L-a)-1)}{30L}.$$

Theorem 3 *Assume that the* $M\times N$ *image* f *is the realization of a discrete iid random vector* $(X_i)_{i=1}^n$ *with iid components* X_i *as* X, *where* $n=MN$. *Let* ν_f *be defined as in* (14) *with respect to* $\mathcal{N}4$. *Then the probability that* $\nu_f\geq a>0$ *is not smaller than*

$$1-(1-2q(X,4,a))^m, \tag{24}$$

where q *is defined as in* (23) *and* $m=\lfloor M/3\rfloor\times\lfloor N/3\rfloor$.

For $\mathcal{N}8$ we have to replace q by $\tilde{q}(X,4,a) := \sum_{i=0}^{L-1} \left(P(X \leq i-a)\right)^4 \left(P(X \leq i-\sqrt{2}a)\right)^4 P(X=i)$.

Proof. We consider only inner pixels i with non-overlapping neighborhoods as depict in Fig. 6. Then, by Lemma 3, the probability that one of these pixels does not fulfill (22) is given by $1-2q(X,4,a)$. Hence the probability that all these inner pixels do not fulfill (22) is $(1-2q(X,4,a))^m$ and the probability that at least one of these pixel fulfills (22) is $1-(1-2q(X,4,a))^m$. □

Note that for $q(X,4,a) > 0$ the probability in (24) is indeed very near to 1 even for moderate sizes of m.

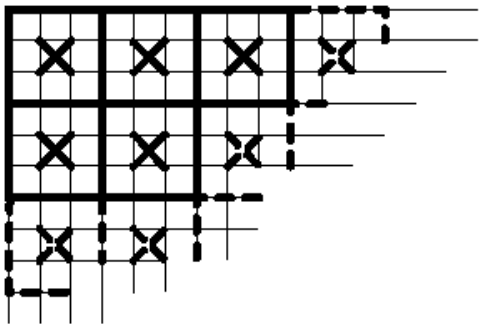

Figure 6: Disjoint 3×3-adjacencies with center pixels 'x'.

6 Numerical Tests

The bounds on $\|\hat{u}-f\|_\infty$ with respect to the model parameters were tested on a wide amount of images. Here we present the results on 15 images of different sizes, with gray values in $\{0,\cdots,255\}$, available at http://sipi.usc.edu/database/. In our selection the images have various quality and content (presence or quasi-absence of edges, textures, nearly flat regions). They are displayed in Fig. 7. The values of ν_f for $\mathcal{N}8$ under each image shows that the assumption $\nu_f - 2b(\beta,\alpha_1) > 0$ in Theorem 2 is generously satisfied in all these cases as far as we are interested to fix $b(\beta,\alpha_1) \leqslant 0.5$.

We tested two functionals $J(\cdot,f)$ as described in Section 2: the first corresponds to $\psi = \Theta 1$ and $\varphi = \Theta 1$ and the second—to $\psi = \Theta 2$ and $\varphi = \Theta 1$ as given in Table 1. In all tests, $\mathcal{N}8$ was adopted with the weights $\gamma_{i,j}$ given in (4). Two choices for β satisfying (19) were considered along with different values for α_1 and α_2. The minimizers $\hat{u}$ were computed using Polak-Ribière conjugated gradients [3] with high numerical precision. For each restored image we computed $\|\hat{u}-f\|_\infty$ and present either the latter norm or how far its value is from the theoretical bound $b(\beta,\alpha_1)$:

$$b(\beta,\alpha_1) - \|\hat{u}-f\|_\infty \ .$$

The tables show also the difference between the upper and the lower theoretical bounds on $\|\hat{u}-f\|_\infty$,

$$b-\ell := b(\beta,\alpha_1) - \ell(\beta,\alpha_1,\alpha_2,\nu_f) \ ,$$

computed using the explicit formulae given in Section 4. Furthermore, we evaluate the amount of pixels that closely approach the ℓ_∞ norm:

$$q = \sharp\left\{ i \in \mathbb{I}_n \;\middle|\; \|\hat{u}-f\|_\infty - |\,\hat{u}[i]-f[i]\,| < \varepsilon \right\} \quad \text{and} \quad Q\% = 100\,\frac{q}{n} \ ,$$

where $\varepsilon \gtrapprox 0$ in order to account for numerical errors. In the experiments, we set $\varepsilon := 10^{-3}$.

In all tests, given $0 < \beta < 1/\eta$, we fixed α_1 so that

$$b(\beta,\alpha_1) = \frac{1}{2} \ .$$

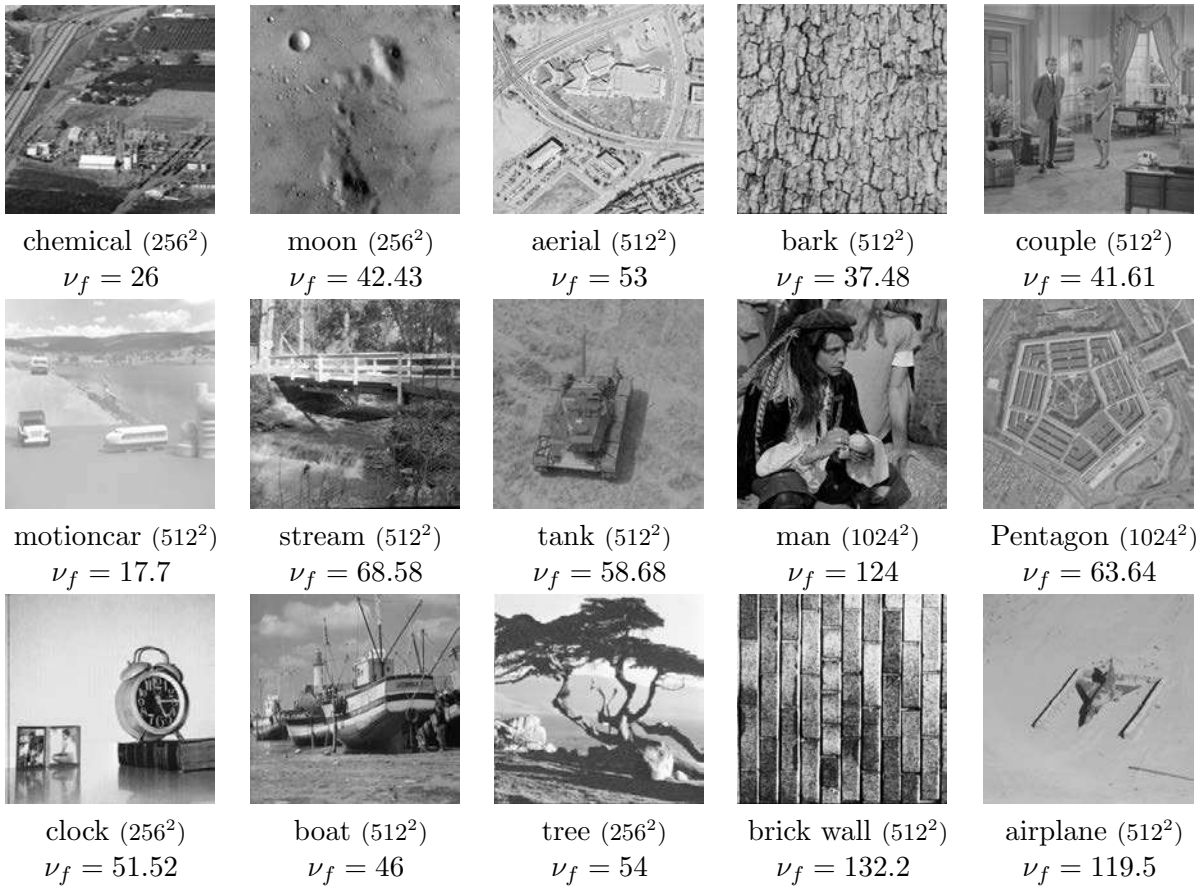

chemical (256^2) $\nu_f = 26$ | moon (256^2) $\nu_f = 42.43$ | aerial (512^2) $\nu_f = 53$ | bark (512^2) $\nu_f = 37.48$ | couple (512^2) $\nu_f = 41.61$

motioncar (512^2) $\nu_f = 17.7$ | stream (512^2) $\nu_f = 68.58$ | tank (512^2) $\nu_f = 58.68$ | man (1024^2) $\nu_f = 124$ | Pentagon (1024^2) $\nu_f = 63.64$

clock (256^2) $\nu_f = 51.52$ | boat (512^2) $\nu_f = 46$ | tree (256^2) $\nu_f = 54$ | brick wall (512^2) $\nu_f = 132.2$ | airplane (512^2) $\nu_f = 119.5$

Figure 7: The set of images used in the tests provided in this section. The values of ν_f are computed according to (14) in the case $\mathcal{N}8$ for the weights in (4).

$\mathcal{N}8$, $\psi(t) = \sqrt{t^2 + \alpha_1}$ for $\alpha_1 = 0.2862$, $\varphi(t) = \sqrt{t^2 + \alpha_2}$ and $\beta = 0.1$

	$\alpha_2 = 0.02$			$\alpha_2 = 100$		
image	$(b-\|\hat{u}-f\|_\infty)\mathbf{10^{-6}}$	$(b-\ell)\mathbf{10^{-6}}$	$Q\,\%$	$\|\hat{u}-f\|_\infty\mathbf{10^{-1}}$	$(b-\ell)\mathbf{10^{-2}}$	q
chemical	4.764	14.90	4.04	4.772	6.143	2
moon	2.438	5.459	9.27	4.875	2.525	1
aerial	2.066	3.465	3.46	4.931	1.647	1
bark	2.977	7.041	6.57	4.866	3.188	1
couple	2.485	2.568	3.25	4.872	2.619	4
motioncar	19.98	33.68	0.18	4.224	11.35	1
stream	0.918	2.051	7.14	4.946	0.995	2
tank	1.960	2.815	6.95	4.907	1.351	1
man	0.025	0.619	4.94	4.984	0.307	8
Pentagon	1.181	2.388	9.12	4.936	1.153	1
clock	2.079	3.671	2.88	4.931	1.740	1
boat	1.707	4.626	6.04	4.916	2.164	2
tree	1.202	3.325	5.27	4.920	1.584	1
brick wall	0.334	0.544	11.8	4.982	0.270	43
airplane	0.412	0.667	1.73	4.979	0.330	1

Table 4: Results for $\psi = \Theta 1$, $\varphi = \Theta 1$, $\beta = 0.1$ and a small and large value of α_2, respectively. Over the whole set of these images, for $\alpha_2 = 0.02$ we have $\text{mean}\big(0.5 - \|\hat{u} - f\|_\infty\big) = 2.968 \times 10^{-6}$ and $\text{mean}\big(0.5 - \ell(\beta, \alpha_1, \alpha_2, \nu_f)\big) = 6.0678 \times 10^{-6}$. For $\alpha_2 = 100$ these values read $\text{mean}\big(0.5 - \|\hat{u} - f\|_\infty\big) = 1.307 \times 10^{-2}$ and $\text{mean}\big(0.5 - \ell(\beta, \alpha_1, \alpha_2, \nu_f)\big) = 2.491 \times 10^{-2}$.

$\mathcal{N}8$, $\psi(t) = \sqrt{t^2 + \alpha_1}$ for $\alpha_1 = 1.895$, $\varphi(t) = \sqrt{t^2 + \alpha_2}$ and $\beta = 0.05$

	$\alpha_2 = 0.02$			$\alpha_2 = 100$		
image	$(b - \|\hat{u} - f\|_\infty)\mathbf{10^{-6}}$	$(b - \ell)\mathbf{10^{-6}}$	$Q\,\%$	$\|\hat{u} - f\|_\infty \mathbf{10^{-1}}$	$(b - \ell)\mathbf{10^{-2}}$	q
chemical	2.561	9.055	4.54	4.858	3.993	2
moon	1.580	3.300	10.2	4.924	1.572	1
aerial	0.872	2.093	3.92	4.958	1.015	2
bark	1.673	4.254	6.82	4.918	2.000	1
couple	1.642	3.432	3.25	4.922	1.632	4
motioncar	12.39	20.35	0.28	4.486	7.847	1
stream	0.727	1.240	7.19	4.967	0.608	3
tank	1.020	1.701	8.31	4.943	0.829	1
man	0.162	0.374	6.00	4.990	0.186	11
Pentagon	0.871	1.442	10.2	4.961	0.706	1
clock	1.013	2.220	2.88	4.958	1.073	1
boat	0.799	2.795	7.14	4.949	1.342	2
tree	0.993	2.009	6.06	4.951	0.975	2
brick wall	0.125	0.329	11.9	4.989	0.164	99
airplane	0.228	0.403	3.48	4.987	0.200	1

Table 5: Results for $\psi = \Theta 1$, $\varphi = \Theta 1$, $\beta = 0.05$ and a small and large value of α_2, respectively. For $\alpha_2 = 0.02$ we have $\text{mean}\big(0.5 - \|\hat{u} - f\|_\infty\big) = 1.777 \times 10^{-6}$ and $\text{mean}\big(0.5 - \ell(\beta, \alpha_1, \alpha_2, \nu_f)\big) = 3.666 \times 10^{-6}$. For $\alpha_2 = 100$, we find $\text{mean}\big(0.5 - \|\hat{u} - f\|_\infty\big) = 0.827 \times 10^{-2}$ and $\text{mean}\big(0.5 - \ell(\beta, \alpha_1, \alpha_2, \nu_f)\big) = 1.610 \times 10^{-2}$.

$\mathcal{N}8$, $\psi(t) = |t| - \alpha_1 \log\left(1 + \dfrac{|t|}{\alpha_1}\right)$ for $\alpha_1 = 0.9645$, $\varphi(t) = \sqrt{t^2 + \alpha_2}$ and $\beta = 0.05$

	$\alpha_2 = 0.05$			$\alpha_2 = 100$		
image	$(b - \|\hat{u} - f\|_\infty)\mathbf{10^{-6}}$	$(b - \ell)\mathbf{10^{-6}}$	$Q\,\%$	$\|\hat{u} - f\|_\infty \mathbf{10^{-1}}$	$(b - \ell)\mathbf{10^{-2}}$	q
chemical	0.101	0.304	2.79	4.811	5.236	2
moon	5.347	11.06	7.03	4.898	2.090	1
aerial	2.670	7.019	2.63	4.943	1.354	2
bark	5.843	14.26	5.55	4.890	2.653	1
couple	5.369	11.51	3.25	4.895	2.170	4
motioncar	41.36	68.23	0.09	4.330	0.101	1
stream	1.687	4.155	6.66	4.956	0.813	3
tank	3.869	5.703	4.45	4.924	1.107	1
man	0.673	1.255	3.14	4.987	0.249	10
Pentagon	2.723	4.837	6.55	4.948	0.943	1
clock	2.622	7.437	2.88	4.944	1.431	1
boat	3.879	9.373	3.97	4.931	1.786	2
tree	4.070	6.737	4.18	4.935	1.301	2
brick wall	0.721	1.102	11.3	4.985	0.219	61
airplane	0.682	1.352	0.74	4.983	0.268	1

Table 6: Results for $\psi = \Theta 2$, $\varphi = \Theta 1$, $\beta = 0.05$ and a small and large value of α_2, respectively. For $\alpha_2 = 0.05$ we have $\text{mean}\big(0.5 - \|\hat{u} - f\|_\infty\big) = 5.441 \times 10^{-6}$ and $\text{mean}\big(0.5 - \ell(\beta, \alpha_1, \alpha_2, \nu_f)\big) = 10.29 \times 10^{-6}$. For $\alpha_2 = 100$, we find $\text{mean}\big(0.5 - \|\hat{u} - f\|_\infty\big) = 1.09 \times 10^{-2}$ and $\text{mean}\big(0.5 - \ell(\beta, \alpha_1, \alpha_2, \nu_f)\big) = 2.11 \times 10^{-2}$.

mean $\big(b(\beta,\alpha_1)-\ell(\beta,\alpha_1,\alpha_2,\nu_f)\big)$, $b(\beta,\alpha_1)=0.5$, $\mathcal{N}8$

	$\alpha_2=0.01$		$\alpha_2=100$	
	$\beta=0.1$	$\beta=0.05$	$\beta=0.1$	$\beta=0.05$
$\psi=\Theta 1$, $\varphi=\Theta 1$	3.034×10^{-6}	1.833×10^{-6}	2.491×10^{-2}	1.610×10^{-2}
$\psi=\Theta 2$, $\varphi=\Theta 1$	5.106×10^{-6}	2.459×10^{-6}	3.985×10^{-2}	2.112×10^{-2}
$\psi(t)=\frac{1}{\alpha_1+1}\lvert t\rvert^{\alpha_1+1}$, $\varphi=\Theta 1$	2.994×10^{-6}	1.045×10^{-6}	2.542×10^{-2}	0.941×10^{-2}

Table 7: The mean value of the difference $b(\beta,\alpha_1)-\ell(\beta,\alpha_1,\alpha_2,\nu_f)$ was computed over the selection of images shown in Fig. 7. Here we consider the $\mathcal{N}8$ neighborhood for the weights in (4).

mean $\big(b(\beta,\alpha_1)-\ell(\beta,\alpha_1,\alpha_2,\nu_f)\big)$, $b(\beta,\alpha_1)=0.5$, $\mathcal{N}4$

	$\alpha_2=0.01$		$\alpha_2=100$	
	$\beta=0.2$	$\beta=0.1$	$\beta=0.2$	$\beta=0.1$
$\psi=\Theta 1$, $\varphi=\Theta 1$	2.980×10^{-6}	1.278×10^{-6}	2.253×10^{-2}	1.104×10^{-2}
$\psi=\Theta 2$, $\varphi=\Theta 1$	5.364×10^{-6}	1.788×10^{-6}	3.780×10^{-2}	1.504×10^{-2}
$\psi(t)=\frac{1}{\alpha_1+1}\lvert t\rvert^{\alpha_1+1}$, $\varphi=\Theta 1$	3.333×10^{-6}	0.812×10^{-6}	2.718×10^{-2}	0.722×10^{-2}

Table 8: The neighborhood here is $\mathcal{N}4$ with the weights given in (4). The mean is calculated over the set of images in Fig.7.

The numerical outcomes confirm the theoretical results on $\|\hat{u}-f\|_\infty$ established in Sections 3 and 4. From Tables 4, 5 and 6 the following observations are drown:

- Decreasing $\alpha_2>0$ towards 0 enables to make the difference between the upper and the lower bounds on $\|\hat{u}-f\|_\infty$ arbitrarily small, so that $\|u-f\|_\infty \lessapprox b(\beta,\alpha_1)$.

  In this case an important percentage of the pixels meet $\|u-f\|_\infty$.

- An important increase of $\alpha_2>0$ entails a minor decrease of the lower bound $\ell(\beta,\alpha_1,\alpha_2,\nu_f)$ but then the number of pixels that are close to $\|u-f\|_\infty$ is reduced to a few ones.

  Such a situation may be preferable when one wishes that there is not a large amount of pixels close to the upper bound.

Tables 7 and 8 show yet again that the gap between the upper bound $b(\beta,\alpha_1)$ and the lower bound $\ell(\beta,\alpha_1,\alpha_2,\nu_f)$ vanishes when α_2 is close to zero and that it increases when α_2 increases. For α_2 fixed, we see that $b(\beta,\alpha_1)-\ell(\beta,\alpha_1,\alpha_2,\nu_f)$ tends to decrease along with β.

Fig. 8 shows the histograms of the differences $\{f[i]-\hat{u}[i],\ i\in\mathbb{I}_n\}$ relevant to "moon", where the upper bound was set to $b(\beta,\alpha_1)=0.5$, for an increasing set of values of α_2. These histograms were plotted for 100 bins equally distributed on $[-0.5,+0.5]$. For very small values of α_2, there are many pixels meeting $|f[i]-\hat{u}[i]|\approx\|f-\hat{u}\|_\infty$. When α_2 increases, such pixels become more and more rare and the differences $|f[i]-\hat{u}[i]|$ become centered near zero. However they never reach zero: see the value of μ defined in the caption of the figure. Here again, numerical test were done with a high precision.

7 Conclusions and Open Questions

L_1-TV functionals have been often minimized using a smoothed version of the form we consider in this paper with ad hoc chosen smoothing parameters ("very small"). The results established in our work enable to clearly evaluate the resulting approximation.

The functions (ψ,φ) studied here have a lot of similarities. However, they produce different image restorations. The question of what couple of functions (ψ,φ) would give a better result in the framework of a given application, remains open.

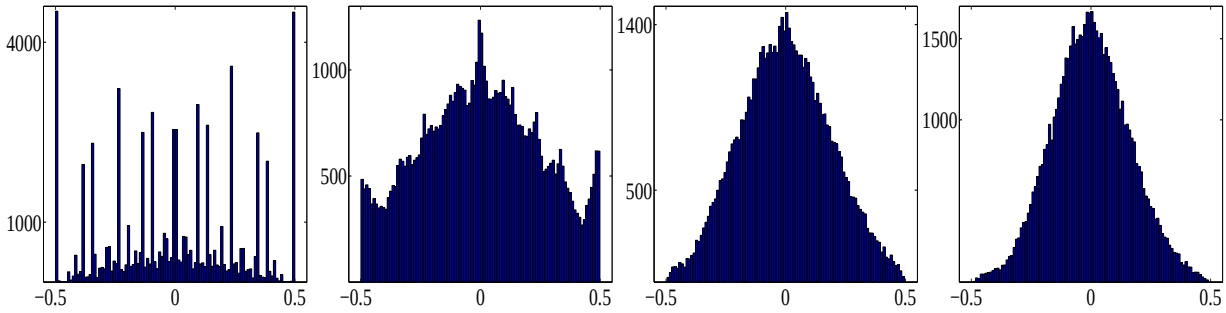

$\alpha_2 = 0.02$, $q = 6700$ $\mu = 6.6 \times 10^{-9}$ | $\alpha_2 = 5$, $q = 48$ $\mu = 5.556 \times 10^{-8}$ | $\alpha_2 = 50$, $q = 3$ $\mu = 1.523 \times 10^{-6}$ | $\alpha_2 = 100$, $q = 1$ $\mu = 2.249 \times 10^{-6}$

Figure 8: Histograms of $\{f[i] - \hat{u}[i],\ i \in \mathbb{I}_n\}$ for "moon" restored using $\psi = \Theta 1$, $\varphi = \Theta 1$, $\mathcal{N}8$, $\beta = 0.05$ and for different values of α_2. The parameter $\alpha_1 = 1.8947$ was set so that $b(\beta, \alpha_1) = 0.5$. The image has $n = 65536$ pixels. The value μ is defined by $\mu := \min_{i \in \mathbb{I}_n} |f[i] - \hat{u}[i]|$.

Extension to the rotational-invariant (in a discrete sense) smoothed TV, i.e. $\Phi(u) = \sum_{i,j} \varphi(\|\nabla_{i,j} u\|)$, where $\nabla_{i,j} u \in \mathbb{R}^2$ stands for a discrete approximation of the gradient of u at pixel (i, j), deserves attention.

Extensions to cases when f are the coefficients of the expansion of the input image using a frame transform is important.

Applications to quantization noise reduction should be envisaged.

References

[1] G. Aubert and P. Kornprobst, *Mathematical problems in image processing*, Springer-Verlag, Berlin, 2 ed., 2006.

[2] M. Black and A. Rangarajan, *On the unification of line processes, outlier rejection, and robust statistics with applications to early vision*, International Journal of Computer Vision, 19 (1996), pp. 57–91.

[3] J. F. Bonnans, J.-C. Gilbert, C. Lemaréchal, and C. A. Sagastizábal, *Numerical Optimization (Theoretical and Practical Aspects)*, Springer, Berlin ; New York NY ; Hong Kong, 2003.

[4] T. Chan and S. Esedoglu, *Aspects of total variation regularized l^1 function approximation*, SIAM Journal on Applied Mathematics, 65 (2005), pp. 1817–1837.

[5] T. Chan and P. Mulet, *On the convergence of the lagged diffusivity fixed point method in total variation image restoration*, SIAM Journal on Numerical Analysis, 36 (1999), pp. 354–367.

[6] D. Coltuc and P. Bolon, *Exact histogram specification*, IEEE Transactions on Image Processing, 15 (2006), pp. 1143–1152.

[7] D. Geman and G. Reynolds, *Constrained restoration and recovery of discontinuities*, IEEE Transactions on Pattern Analysis and Machine Intelligence, PAMI-14 (1992), pp. 367–383.

[8] M. Nikolova, , *Analytical bounds on the minimizers of least squares*, Inverse Problems in Imaging 1(4) (2007), pp. 661–677.

[9] M. Nikolova, Y.-W. Wen, and R. Chan, *Exact histogram specifcation for digital images using a variational approach*, Tech. Report, CMLA Report N. 2012-01, ENS Cachan, France, 2012.

[10] Y. Wan and D. Shi, *Joint exact histogram specification and image enhancement through the wavelet transform*, IEEE Transactions on Image Processing, 16 (2007), pp. 2245–2250.

[11] E. Weiszfeld, *Sur le point pour lequel la somme des distances de n points donnes est minimum*, Tôhoku Mathematics Journal 43 (1937), pp. 355–386.

Addresses:
F. Baus
Fraunhofer ITWM
Fraunhofer Platz 1
67663 Kaiserslautern
Germany

M. Nikolova
CMLA
ENS Cachan
CNRS, PRES UniverSud. 61 av. du President Wilson
94235 Cachan Cedex
France
nikolova@cmla.ens-cachan.fr

G. Steidl
University of Kaiserslautern
Department of Mathematics
Paul-Ehrlich-Str. 31
67663 Kaiserslautern
Germany
steidl@mathematik.uni-kl.de